Available online at www.sciencedirect.com
ScienceDirect
Journal of the European Ceramic Society 26 (2006) 3279–3285
www.elsevier.com/locate/jeurceramsoc

Fabrication and characterization of zinc phosphate passivation layers for ZnO-based varistor

W.S. Lee [a,*], W.T. Chen [a], Tony Yang [b], Y.C. Lee [b], C.Y. Su [b], S.P. Lin [b], C.L. Hu [b]

[a] *Department of Electrical Engineering, National Cheng Kung University, Taiwan*
[b] *R&D Technology Center, Yageo Corporation Nantze Branch, Taiwan*

Received 4 February 2005; received in revised form 31 August 2005; accepted 11 September 2005
Available online 22 November 2005

Abstract

The chemical and morphological modification of zinc phosphates as a protection layer for ZnO-based varistor has been made through the addition of Mg or Ca species to the conversion solution combined with the calcinations of zinc phosphates. The results showed that the aspect ratio of as-coated zinc phosphates grains can be greatly reduced through the addition of Mg or Ca species. Moreover, the introduction of calcination to zinc phosphate not only makes the coating layer more dense, smooth, and resistive, but also results in the increase in capacitance, non-linear coefficient (α). On the other hand, loss tangent and breakdown voltage are both slightly decreased with increasing calcination temperatures. The increase in capacitance after calcinations may result from both the re-crystallization of Bi_2O_3-containing grain boundary phase and the reduction of oxygen vacancies.

Keywords: Varistor; Calcination; ZnO; Passivation layers; $Zn_3(PO_4)$

1. Introduction

Doped-ZnO ceramic due to its nonlinear ohmic property and excellent energy handling capability has become one of the promising varistors.[1] The microstructure of ZnO consists of highly conductive n-type ZnO grains, which are surrounded by an electrically insulting grain boundary phases. Due to its semi-conductive characteristic, an insulating layer needs to be selectively deposited on the exposed surface of ZnO varistor but not on the electrically conductive end terminations during the manufacturing of multilayer varistor (MLV). Therefore, this device can be plated by using a conventional plating process. More importantly, the plating only takes place on the end terminations. The insulating layers, such as phosphates, glass, and polymer have been reported.[2–6] The fabrication of phosphates is chemically oriented while that of glass or polymer is more physically oriented. Moreover, it is found that the phosphates will be leached out during Ni or Sn electroplating. The leaching of this insulating layer will result in the change in morphology of passivation layer, reduction of insulation resistance, increased leakage current, increase in loss factor, and permeation of plating solution into ceramics, leading to serious degradation of MLV during operation.[7]

Therefore, the purpose of this work is to chemically modify zinc phosphate [$Zn_3(PO_4)\cdot 4H_2O$] through the conversion treatment and calcinations of the coating layer. The effect of chemical additives on the composition and morphology of $Zn_3(PO_4)\cdot 4H_2O$ will be studied and reported. The relationship between microstructure of zinc phosphates and electrical properties are investigated in dependence of the processing parameters.

2. Experimental procedure

The doped ZnO semiconductors were immersed and made to react with a phosphoric acid solution to form an electrically insulating phosphates coating layer. The passivation process was performed at ambient temperature for a period of time. The pH value of phosphoric acid solution is in the range of 1–5. The as-coated zinc phosphates coating layers were then calcined in the temperature range of 600–850° C under air conditions.

* Corresponding author.
E-mail address: leewen@mail.ncku.edu.tw (W.S. Lee).

0955-2219/$ – see front matter © 2005 Elsevier Ltd. All rights reserved.
doi:10.1016/j.jeurceramsoc.2005.09.085

The insulation resistance (IR) of the samples was measured by using a high resistive meter (4339B, Hewlett-Packard Inc., USA) at an applied voltage of 1 V/s. The phase of zinc phosphate was determined by using X-ray diffractometer (X'pert, Philips Instrument Inc., Netherlands). The microstructures of the specimens were characterized by scanning electron microscope (Leo 1530, Philips Instrument Inc., Netherlands or JSM-5300, JEOL, Japan) equipped with an energy-dispersive spectrometer (EDS, EDAX Inc., USA).

3. Results and discussion

Fig. 1 shows the SEM micrograph of ZnO-based varistor. The image shows that some $Zn_7Sb_2O_{12}$ (ZS) spinel particles are incorporated into the ZnO grains while others are distributed in the matrix. It is reported that Bi_2O_3 and Sb_2O_3 react with ZnO to form $Bi_3ZnSb_3O_{14}$ (BZS), which transforms to ZS at 950–1050° C upon slow cooling.[8,9] The pyrochlore phase is undesirable because it shows no nonlinear ohmic behavior. It is believed that the incorporation of smaller ZS particles to the interior of ZnO grains may result from the faster migration of Bi_2O_3-containing grain boundary phase during co-firing. Besides, the Bi_2O_3 segregates to Ag–Pd inner electrodes and then reacts with Pd to give Bi–Pd–O phases. The results are consistent with literature.[10]

Fig. 2 shows the XRD spectra of the as-coated zinc phosphates. The result shows that the crystalline phase of zinc phosphate is similar when reacting at 35 and 70° C, respectively. Note that the powders are dried at 150° C/2 h for the ease of powder handling. Therefore, partially dehydration of zinc phosphate takes place and the phases are indexed as $Zn_3(PO_4)\cdot 2H_2O$. However, different crystalline phases, as shown in Fig. 3, are obtained after calcining at 785° C/10 min. The zinc phosphate, reacted at 35° C is hopeite phase while that reacted at 70° C is phosphophyllite phase. The occurrence of different zinc phosphates is reported in literature.[11]

Fig. 4 shows the SEM micrographs of the as-coated zinc phosphate, made to react at 35 and 70° C, respectively. Though the crystalline phase of calcined zinc phosphate is different (Fig. 3),

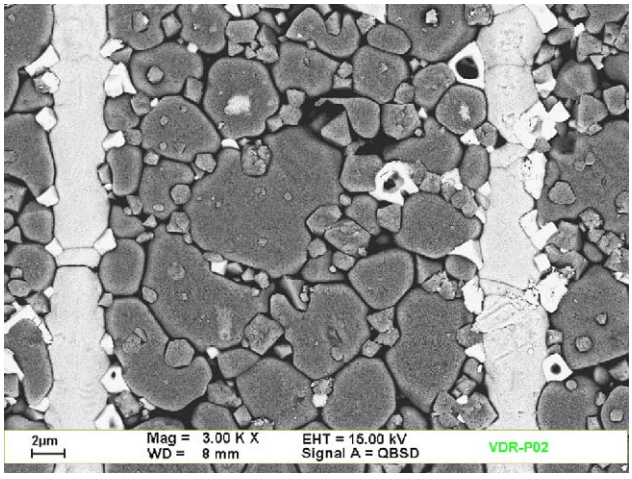

Fig. 1. SEM microstructure of doped-ZnO varistor.

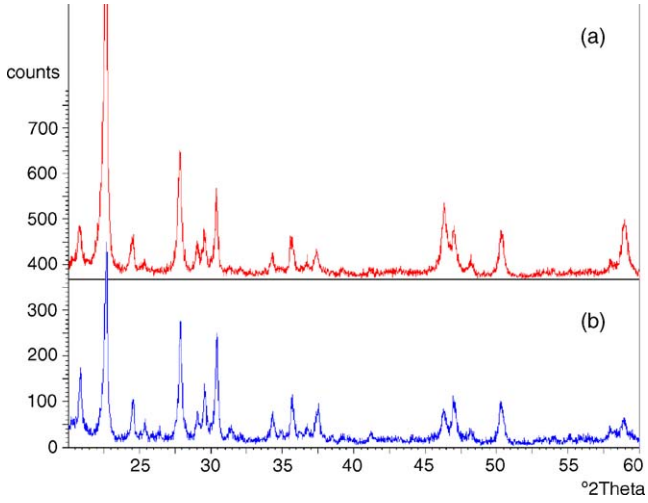

Fig. 2. XRD spectra of as-coated zinc phosphates, which are reacted at (a) 35 and (b) 70 °C for 4 h, respectively.

the SEM morphologies of the as-coated zinc phosphates are quite similar. Platy grains are formed and the aspect ratio is ≥10. Fig. 5 shows the SEM micrographs of the as-calcined zinc phosphates, which are reacted at 35 and 70° C, respectively. As can be seen in Fig. 4, the coverage of zinc phosphate on the surface of ZnO is not complete. After calcining at 785° C/10 min, a smooth, dense, and strong adhesion protection layer with high resistivity can be obtained. The platy grains disappear, partially melt, and flow into the interstices of uncovered regions during calcination. The calcination of zinc phosphate not only results in the morphology change from platy grains to spherical grains but also leads to the improved physical and electrical properties. It is believed that the densification of zinc phosphate may take place through the viscous flow mechanism.

Fig. 6 shows a series of SEM micrographs of zinc phosphates, which are calcined in the temperature range of 650–800° C for 10 min. The images show that the morphologies of platy grains start to change when calcining at 650° C. The significant changes

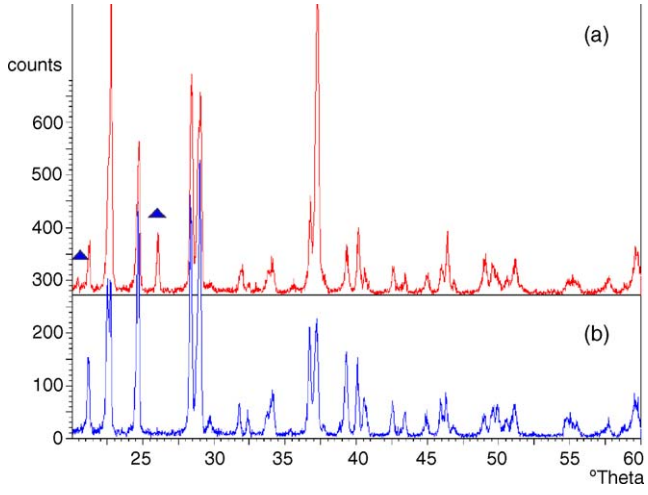

Fig. 3. XRD spectra of zinc phosphates, which are reacted at (a) 35 and (b) 70 °C, respectively. After conversion treatment, the zinc phosphates are calcined at 785 °C/10 min.

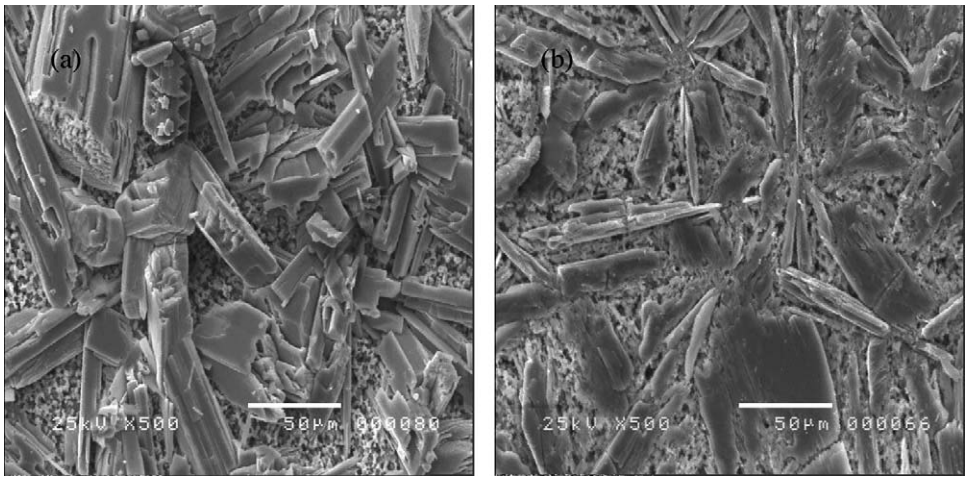

Fig. 4. SEM micrographs of the as-coated zinc phosphates reacted at (a) 35 °C and (b) 70 °C for 4 h, respectively.

in the morphologies of grains can be observed after calcining at 700° C. Most of the platy grains disappear and exhibit spherical grains with some flow pattern of grains, as shown in Fig. 6(b). The residual flow patterns can still be observed at the calcination temperature of 750° C. The dense, smooth, and highly resistive protection layer, consisting of zinc phosphates, can be obtained when calcining in the temperature range of 750–800° C.

It is reported that Mg- or Ca-doping can modify the morphology of zinc phosphates and may improve the leaching resistance of zinc phosphates during electroplating.[12,13] The as-coated and as-calcined microstructures of Mg-doped zinc phosphates are shown in Fig. 7, respectively. The aspect ratio of as-coated grains decreases dramatically with the addition of Mg species. The aspect ratio of Mg-doped zinc phosphates is estimated to be $\leq$5.0. More uniform microstructures can be obtained as the addition of Mg increases upto 0.3 wt%, based on the base conversion solution. The similar microstructures can be found in the case of Ca-doped zinc phosphates, as shown in Fig. 8.

The combination of Mg- and Ca-codoped zinc phosphates is also investigated. Fig. 9 shows the SEM micrographs of Mg- and Ca-codoped zinc phosphates, illustrating the formation of platy grains. The aspect ratio of grains can be significantly reduced when added Mg or Ca individually. However, it seems like the occurrence of platy grains takes place when codoped with Mg and Ca species in the conversion bath. Moreover, Fig. 10 demonstrates the comparison of SEM microstructures between undoped and doped zinc phosphates after Sn electroplating. The images show that the leaching resistance of zinc phosphates against the plating solution can be improved through the addition of Mg and Ca species.

While calcination process is conducted to improve the quality of zinc phosphates, the electrical properties, such as capacitance, loss tangent, non-linear coefficient, and breakdown for the ZnO-based MLV with covered zinc phosphates are affected as well and shown in Table 1. Evidently, with increasing calcinations temperature, capacitance and non-linear coefficient are both slightly increased, contrary, loss tangent and breakdown voltage are both significantly decreased. Without the calcination process, the loss tangent of ZnO-based MLV is 3.81%, with increasing calcinations temperature from 650 to 800 °C, the loss tangent of ZnO-based MLV is decreased from 3.67 to 3.2%. Assuming that the hopping of the trapped electrons

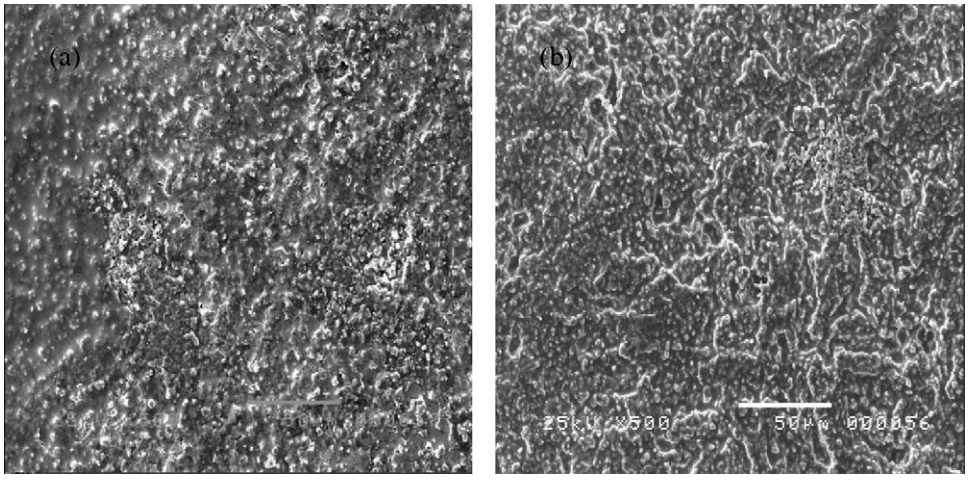

Fig. 5. SEM micrographs of zinc phosphates, calcined at 785 °C/10 min. The conversion treatment was performed at (a) 35 °C and (b) 70 °C, respectively.

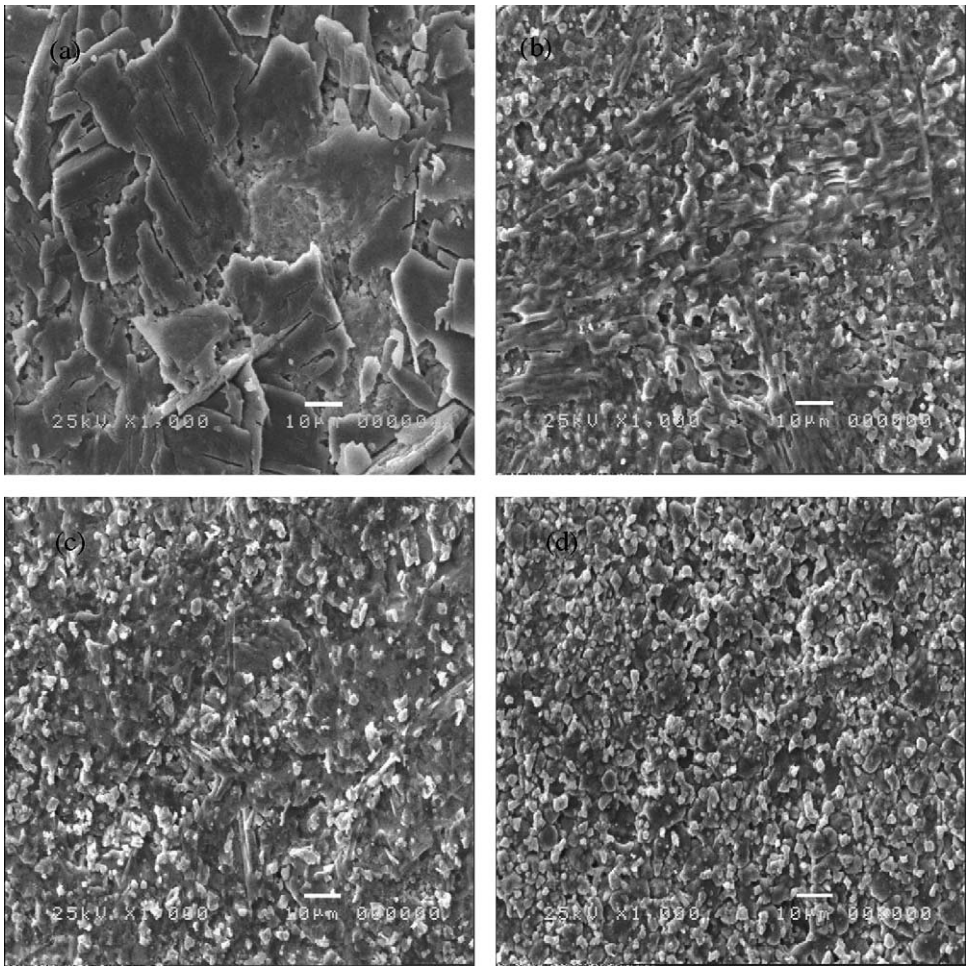

Fig. 6. SEM microstructures of zinc phosphate, calcined in the temperature range of (a) 650, (b) 700, (c) 750, and (d) 800 °C for 10 min.

from the occupied to the unoccupied state that happened during calcinations process is response for the change of loss tangent.[14]

As the calcination temperature increases, non-linear coefficient is slightly increased from 18.7 without calcinations to 23.4 with calcinations at 800 °C for 30 min. It has been mentioned to change the shape of E–J curves by a post-sintering heat treatment.[15] According to a previous discussion, the thermal behavior should change if a modification of the width of transition range occurs. The heat treatment broadened the transition region with a respective change of the temperature behavior. The flattening and decrease of E–J curves of samples with calcinations could be explained through the theory of Gupta.[16] According to this theory, migrating interstitial zinc recombines with oxygen atoms, thereby forming thermally stable ZnO at the grain boundary. This reaction should be accompanied by a decrease of grain boundary states and leads to an increase of non-linear coefficient.

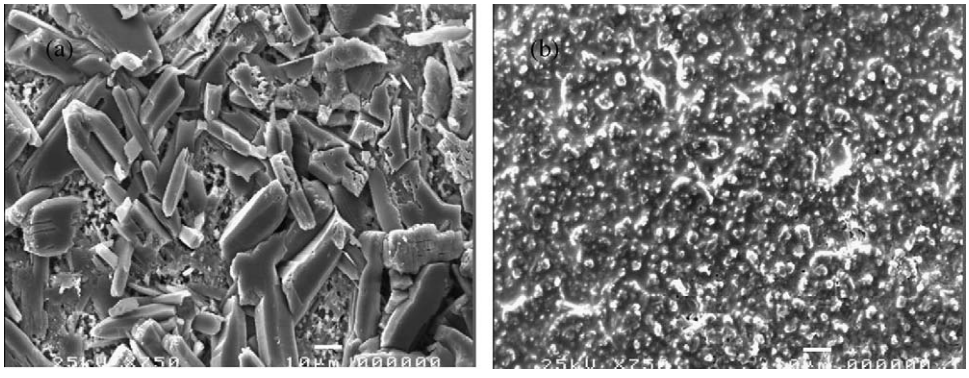

Fig. 7. SEM micrographs of (a) as-coated and (b) as-calcined Mg-doped zinc phosphates.

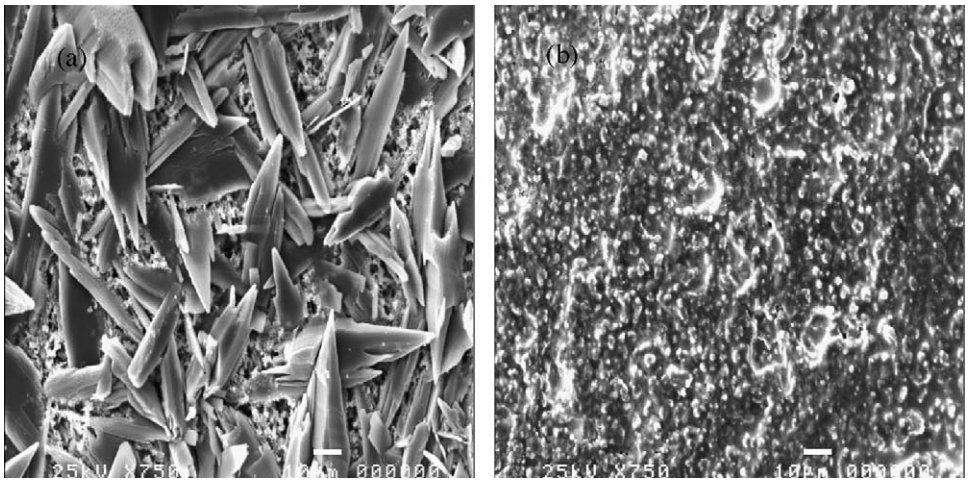

Fig. 8. SEM micrographs of (a) as-coated and (b) as-calcined Ca-doped zinc phosphates.

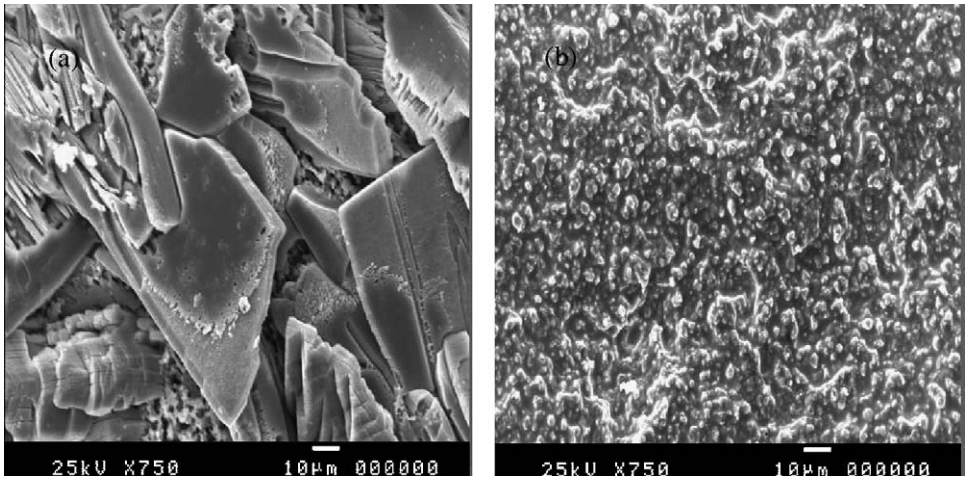

Fig. 9. SEM micrographs of (a) as-coated and (b) as-calcined Mg and Ca codop zinc phosphates.

The reduction of the breakdown voltage with increasing calcinations temperature is associated with the change of microstructure. The high nonlinear voltage-dependent behavior of a ZnO-based MLV is a grain boundary phenomenon. A ZnO-varistor consists of highly conductive (n-doped with Al) ZnO grains, which are separated by a few atom layers of Bi and oxygen. At these interfaces, acceptor states are formed which lead to the formation of a double-Schottky barrier towards the adjacent ZnO

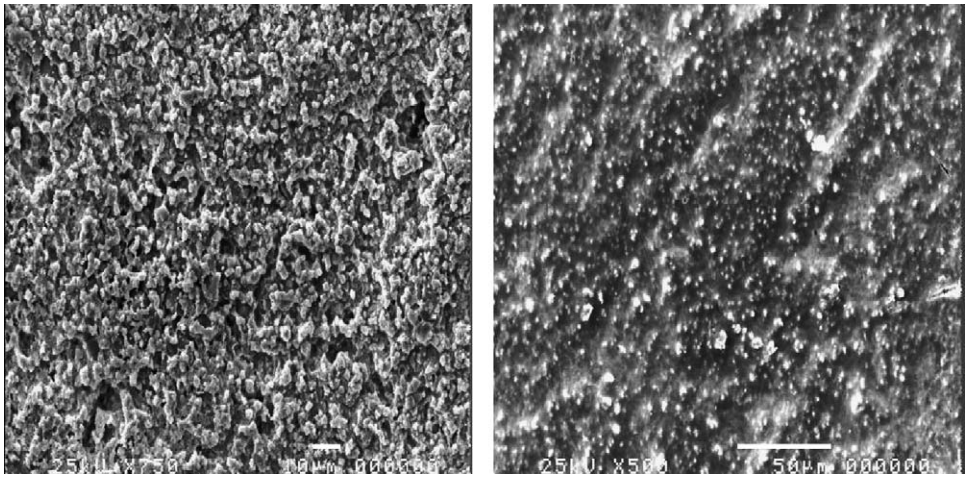

Fig. 10. SEM micrographs of (a) undoped, and (b) Mg and Ca codop zinc phosphates after Sn electroplating.

Table 1
Calcination effect on the electrical properties of ZnO-based MLV covered with zinc phosphate passivation layer

Calcination	Capacitance (pF)	Tan δ	V_B (V)	α
Without	90	3.81%	8.75	18.7
650 °C/30 min	100	3.67%	8.12	21.7
700 °C/30 min	107	3.49%	8	21.6
750 °C/30 min	120	3.32%	7.8	21.8
800 °C/30 min	118	3.20%	7.85	23.4

grains.[17] Consequently, each grain acts as a potential barrier with a breakdown voltage of about 3 V. The individual breakdown voltages of all grain boundaries, which form the current path between the external electrodes, add up to the total breakdown voltage of the varistor.

$$V = N_{GB} \times V_{GB} = \frac{D}{d_g} V_{GB} \quad (1)$$

With the number of grain boundaries being N_{GB}, the breakdown voltage per grain boundary V_{GB}, the electrode distance D, and the diameter of average grain size d_g. As a consequence, the breakdown voltage for a multilayer varistor can be controlled by changing the grain size or the electrode distance. In the study on the calcination effect, electrode distance is kept same, grain size would be a main factor to influence on the breakdown voltage of ZnO-based MLV with covered zinc phosphates. High calcination temperature is the result of the grain growth of ZnO-based MLV. As we know, the average grain size of a varistor is inversely proportional to the breakdown field. Usually, a small grain size will lead to a big V_B

An interesting phenomenon is observed after calcining the zinc phosphate at 785 °C/30 min. It is found that the calcinations profile affects the capacitance of ZnO varistor. The variation of capacitance of varistor as a function of calcinations profile is shown in Fig. 10. A slow cooling rate (CP01) is used while a quenching rate (CP02) is adopted. The capacitance increases with the calcination temperatures up to 800 °C. Also, a slow cooling rate seems to have a higher increase in capacitance.

The AC impedance of ZnO-based varistor is measured and plotted in Fig. 11. The result shows that different grain boundary behaviors are seen in the Cole–Cole plot. It is well known that the grain boundary phenomenon of ZnO varistor, resulting from the formation of a potential barrier in the presence of dopants

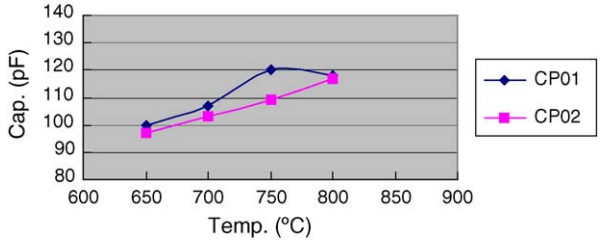

Fig. 11. Capacitance as a function of calcination temperature.

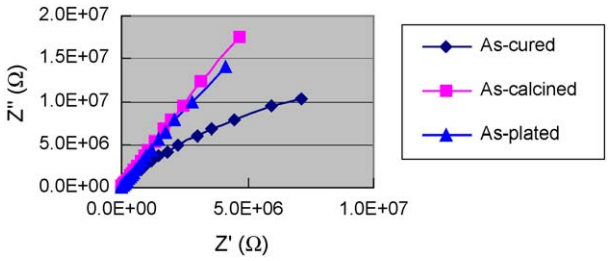

Fig. 12. Cole–Cole plot of varistor, illustrating the differences in grain boundary conductivity after different treatments.

dominates the electrical properties of doped ZnO varistor.[18,19] The calcination of zinc phosphates not only results in the densification of zinc phosphates but also changes the microstructures of ZnO varistor. Fig. 12 shows the SEM image of ZnO-based varistor, illustrating the segregation and re-crystallization of Bi_2O_3-containing grain boundary phases. The calcination makes the Bi_2O_3-rich grain boundary phases more crystalline, which may lead to a higher electrical resistivity of the grain boundary phase. As can be seen in Fig. 11, only one semicircle can be observed, demonstrating that the electrical properties of ZnO are only controlled by Bi_2O_3-containing grain boundary phase. Therefore, we propose that the segregation and re-crystallization of Bi_2O_3-rich grain boundary phase may contribute to the enhancement in the increase in capacitance (Fig. 13).

Moreover, the cooling rate seems to play a role in the increase of capacitance of ZnO varistor, as shown in Fig. 10. A slower cooling rate may allow the removal of oxygen vacancy, leading to the reduction of oxygen vacancy when compared to a faster cooling rate. In complex-impedance plane, it is reported that the relaxation may be associated with the singly ionized oxygen vacancy (V_O').[20,21] The reduction of oxygen vacancy will reduce the concentration of the charge carriers, resulting in the increase in electrical resistivity, as can be observed in Fig. 11. The enhancement of capacitance may be due to the reduction of oxygen vacancy.

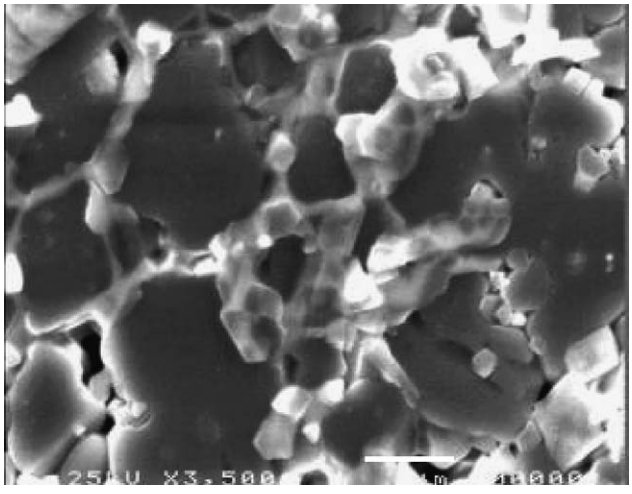

Fig. 13. SEM micrograph of varistor, showing the segregation of glassy phase to the grain boundary.

4. Conclusions

The conclusion of this work is as follows.

1. The microstructure of doped ZnO varistor has been characterized. The formation of ZS either in the intra- or intergranular particles are observed. The segregation of Bi_2O_3 to Ag–Pd inner electrode and reaction of Bi_2O_3 with Pd are noted.
2. The passivation layer, consisting of zinc phosphate on the surface of ZnO-based varistor is successfully made. No significant crystalline phases can be found, reacted at either 35 or 70 °C. However, different crystalline phases are obtained after calcinations. Moreover, the chemical and morphological modification of zinc phosphates through the addition of Mg or Ca species to the conversion solution is done. Shorter aspect ratio of grains can be obtained in Mg- or Ca-doped zinc phosphates. Moreover, the leaching resistance of the protection layer against plating solution can be significantly enhanced.
3. The introduction of calcinations to zinc phosphates not only results in a dense, smooth, and high resistive protection layer, but also results in the increase in capacitance, non-linear coefficient (α). On the other hand, loss tangent and breakdown voltage are both slightly decreased with increasing calcinations temperature. The enhancement of capacitance after calcinations may result from both the re-crystallization of Bi_2O_3-containing grain boundary phase and the reduction of oxygen vacancies.

Acknowledgement

The authors would like to thank the financial support from National Science Council under grant No. NSC-94-2213-E006-048.

References

1. Fayat, J. and Castro, M. S., Defect profile and microstructural development in SnO_2-based varistors. *J. Eur. Ceram. Soc.*, 2003, **23**, 1585–1591.
2. Clinton, C, Spalding, T. R., Connell, A. M., Barrett, J. and Rohan, J. F. Phosphate coating for varistor and method. U.S. Patent No. 6,214,685.
3. Ravindranathan, P. Zinc phosphate coating for varistor and method. E.P. Patent No. 0 806 780 A1.
4. Shiraishi, K., Inoue, T., Sasaki, R., Noi, K. and Tokunaga, H. Zinc oxide varistor and method of manufacturing same. U.S. Patent 2003/0043013 A1.
5. Tokunaga, H., Higashitani, M. and Wakahata, Y., Method for manufacturing varistor. U.S. Patent No. 6,260,258 B1.
6. Tokunaga, H., Higashitani, M. and Wakahata, Y. Method for manufacturing varistor. U.S. Patent No. 6,262,258.
7. Chen, W. P., Lu, S. G. and Chan, H. L. W., Influence of electroless nickel plating on I–V characteristics and its implications for reliability in ZnO-based ceramic varistors. *Mater. Sci. Eng.*, 2003, **B99**, 70–73.
8. Mergen, A. and Lee, W. E., Microstructural ralations in BZS pyrochlore–ZnO mixtures. *J. Eur. Ceram. Soc.*, 1997, **17**, 1049–1060.
9. Mergen, A. and Lee, W. E., Fabrication and crystal chemistry of $Bi_{3/2}ZnSb_{3/2}O_7$ pyrochlore. *J. Eur. Ceram. Soc.*, 1996, **16**, 1041–1050.
10. Wang, S. F., Dough, J. P., Huel, W. and Pt, J. G., Silver–palladium thick-film conductors. *J. Am. Ceram. Soc.*, 1994, **77**(12), 3051–3070.
11. Frost, R. L., An infrared and raman spectroscopic study of natural zinc phosphates. *Spectrochim. Acta Part A*, 2004, **60**, 1439–1445.
12. Morks, M. F., Magnesium phosphate treatment for steel. *Mater. Lett.*, 2004, **58**, 3316–3319.
13. Aramaki, K., XPS and EPMA studies on self-healing mechanism of a protective film composed of hydrated cerium (III) oxide and sodium phosphate on zinc. *Corros. Sci.*, 2003, **45**, 199–210.
14. Bai, S. N. and Tseng, T. Y., Influence of sintering temperature on electrical properties of ZnO varistor. *J. Appl. Phys.*, 1993, **74**(1), 695–703.
15. Gambino, J. P., Kingery, W. D., Pike, G. E., Philipp, H. R. and Levinson, L. M., Effect of heat treatment on the wetting behavior of bismuth-rich intergranular phases in ZnO:Bi:Co varistors. *J. Am. Ceram. Soc.*, 1989, **72**(4), 642–645.
16. Pike, T. P., Electronic properties of ZnO varistors: the microstructure of a ZnO varistor. *Mater. J. Mater. Soc.*, 1985(20), 4091–4098.
17. Bueno, P. R., de Gassia-Santos, M. R., Leite, E. R. and Longo, E., Nature of the Schottjy-type barrier of highly dense SnO_2 systems displaying nonohmic. *Behav. J. Appl. Phys.*, 2000, **88**(11), 6545–6548.
18. Duran, P., Tartaj, J. and Moure, C., Fully dense, fine-grained, doped zinc oxide varistors with improved nonlinear properties by thermal processing optimization. *J. Am. Ceram. Soc.*, 2003, **86**(8), 1326–1329.
19. Haskell, B. A., Souri, S. J. and Helfand, M. A., Varistor behavior at twin boundaries in ZnO. *J. Am. Ceram. Soc.*, 1999, **82**(8), 2106–2110.
20. Zhou, D. X., Zhang, C. C. and Gong, S. P., Degradation phenomena due to DC bias in low-voltage ZnO varistors. *Mater. Sci. Eng.*, 2003, **B99**, 412–415.
21. Castro, M. S. and Aldao, C. M., Different degradation processes in ZnO varistors. *Ceram. Int.*, 1996, **22**, 39–43.